

Impact of Jamming Attack on Galileo Receivers

Ying-Ren Chien^{1*}, Po-Yu Chen²



¹ Department of Electrical Engineering, National Ilan University, Yilan 260, Taiwan
yrchien@niu.edu.tw

² Storage HW Design Division, Wiwynn Corporation, New Taipei City 221, Taiwan
poyu_chen@wiwynn.com

Received 7 June 2015; Revised 11 July 2015; Accepted 8 December 2016

Abstract. This paper surveys the impact of different jammers on the Galileo receivers in the L1 band. Specifically, we examined the relationship of the sweep-rate of chirp-style jammers with the detection probability when acquiring a Galileo signal. The simulation results show that the relationship between the sweep-rate of the chirp jammers and the resulting impact of the acquisition process is a non-linear function. With the of 45 dB-Hz, the probability of successful acquisition is less than 95% when the sweep rate of the chirp jammer is about 1 GHz/sec and the jamming-to-signal ratio (JSR) is above 21 dB; on the other hand, when the jammer type is the continuous-wave interference, the Galileo receivers can tolerate the JSR of 25 dB.

Keywords: chirp, Galileo, jamming, GNSS

1 Introduction

Recently, the location-based applications have gained great attention. Among many locationing technologies, the Global Positioning System (GPS) technologies are accessible for the civil-oriented navigation system. Furthermore, the European Galileo program has been launched a global navigation satellite system (GNSS) which provides enhanced accuracy. Similar to the GPS receivers, the Galileo receivers need some anti-jamming mechanism to assure the required levels of quality of services (QoS) [1]. Although many anti-jamming techniques have been proposed for GPS receivers, including space domain [2-4], time domain [5-9], and frequency domain [10-13], and time-frequency domain [14, 15], few research results have been reported for Galileo receivers [16]. Moreover, many previous works assumed the jammers are in the continuous-wave interference (CWI) forms. Recently, the chirp-like jammers have been drawn a lot of attention [17-21]. However, these papers are focused on GPS receivers.

This paper provides a numerical analysis of the impact of linear chirp jamming on the acquisition and tracking loops. The simulation results show that the linear chirp jammers have more impact on the Galileo receivers than the CWI jammers. Furthermore, we find that the probability of successful acquisition is a non-linear function of sweep rate of the linear chirp jammers.

2 System Model

The Galileo L₁ band (1559-1592 MHz) signals are the most appealing for consumer electronics and present all unique characteristics of the Galileo signal, such as Binary Offset Carrier (BOC) and Coherent Adaptive Subcarrier Modulation (CASM). The L₁ band Galileo signal includes three channels: *A*, *B*, and *C* channels. The *A* channel contains encrypted data for the public regulated services, while the *B* and *C* channels contain navigation data and the data-less pilot tones, respectively. These channels are modulated through *BOC* modulation. Without loss of generality, we only consider the *B* channel in the L₁ band in this paper.

* Corresponding Author

BOC modulation is usually denoted as $BOC(n, m)$, which means the subcarrier frequency $f_{sc} = n \cdot 1.023$ MHz, and the code rate K MHz. Therefore, the B channel signals, which are $BOC(1, 1)$ modulated, transmitted by the n -th satellite, $y_n(t)$ can be expressed as:

$$y_n(t) = \sqrt{2P_s} e_B(t) \cdot \cos(2\pi f_{L_1} t + \theta) \quad (1)$$

with

$$e_B(t) = \sum_{i=-\infty}^{\infty} C_{L_1-B, [\text{mod}(i, 4092)]} D_{L_1-B, [\text{mod}(i, 4092)]} \times \Pi_{T_c, L_1-B} \cdot \text{sign}[\sin(2\pi R_{c, L_1-B} t)] \quad (2)$$

where P_s is the power of signals; θ is the phase delay; f_{L_1} is the carrier frequency of L_1 (1575.42 MHz); C_{L_1-B} is the spreading code with chip rate R_{c, L_1-B} MHz; D_{L_1-B} is navigation data stream, $\text{mod}\{\cdot\}$ is the modulo operation, $\Pi\{\cdot\}$ is the rectangular function and $\text{sign}\{\cdot\}$ the sign function. Note that, we set the carrier-to-noise ratio C/N_0 as 45 dB-Hz in this paper.

In the presence of interference, the received signals can be modeled as

$$s(t) = \sum_{k=0}^{K-1} y_k(t) + i(t) + w(t) \quad (3)$$

where $y_k(t)$ is the useful signals transmitted by the n -th satellite as defined in (1), K is the number of available satellite for a Galileo receiver, $i(t)$ is the jamming signal and $w(t)$ is the noise term. Due to the orthogonality of the spreading code, a Galileo receiver is able to individually process the signal transmitted by different satellites. Therefore, without loss of generality, the received signal $\tilde{r}(t)$ can be simplified to consider a single satellite at a time. After down conversion to the intermediate frequency (IF), the down-converted signal can be expressed as

$$\tilde{r}(t) = s'(t) + w(t) + i(t) \quad (4)$$

where $s'(t) = \sqrt{2P_s} e_B(t - \tau) \cos[2\pi(f_d + f_{IF})t + \theta]$; τ is the delay introduced by the transmission channel of the satellite; f_d and θ are the corresponding Doppler frequency and the phase offset, respectively; and f_{IF} is the IF of 4.092 MHz. $\tilde{r}(t)$ is then bandpass-filtered and amplified. Therefore, the input signal $r(t)$ at the input of the ADC can be expressed as

$$r(t) = \{[s'(t) + w(t) + j(t)] * h_{BP}(t)\} G(t) \triangleq \tilde{s}(t) + \tilde{w}(t) + \tilde{j}(t) \quad (5)$$

where $h_{BP}(t)$ is the impulse response of the band-pass filter (BPF), and $G(t)$ is the gain of the variable gain amplifier (VGA); "*" denotes the convolution operation. $r(t)$ is then sampled at the rate $1/T_s = 4f_{IF}$.

2.1 Jamming Model

The jamming signals, assumed to be chirp-type or continuous-wave interferences (CWIs), can be expressed as

$$j(t) = \sum_{i=1}^K \sqrt{2P_{J,i}} \cos(2\pi f_{J,i}(t)t + \theta_{J,i}) \quad (6)$$

where K is the number of jammers and $P_{J,i}$, $f_{J,i}(t)$ and $\theta_{J,i}$ are the power, starting frequency (at time $t = 0$), and phase delay of the i^{th} jamming signal, respectively. For different types of jammers, the definition of $f_{J,i}(t)$ can be found in Table 1. Note that f_0 is the initial frequency, t_g is the target time, $f_i(t_g)$ is the instantaneous frequency.

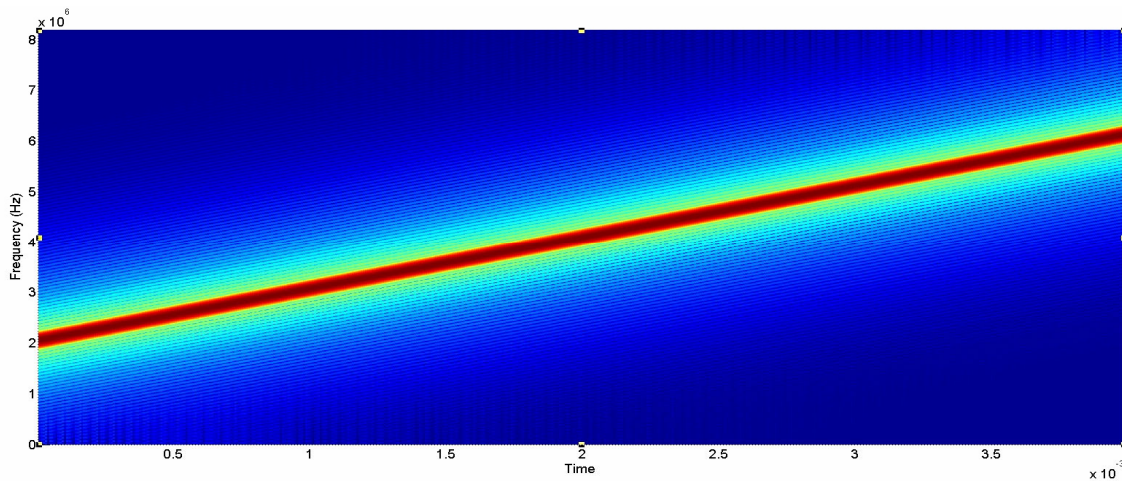
Table 1. The definition of frequency sweep in (6) for different types of jammers

Jamming type	Frequency Sweep $f_{J,i}(t)$	β
Linear chirp	$f_{J,i}(t) = f_0 + \beta t$	$\beta = \frac{f_i(t_g) - f_0}{t_g}$
Convex chirp	$f_{J,i}(t) = f_0 + \beta t^2$	$\beta = \frac{f_i(t_g) - f_0}{t_g^2}$
Logarithmic chirp	$f_{J,i}(t) = f_0 \beta^t$	$\beta = \left(\frac{f_i(t_g)}{f_0} \right)^{\frac{1}{t_g}}$
CWI	$f_{J,i}$	NA

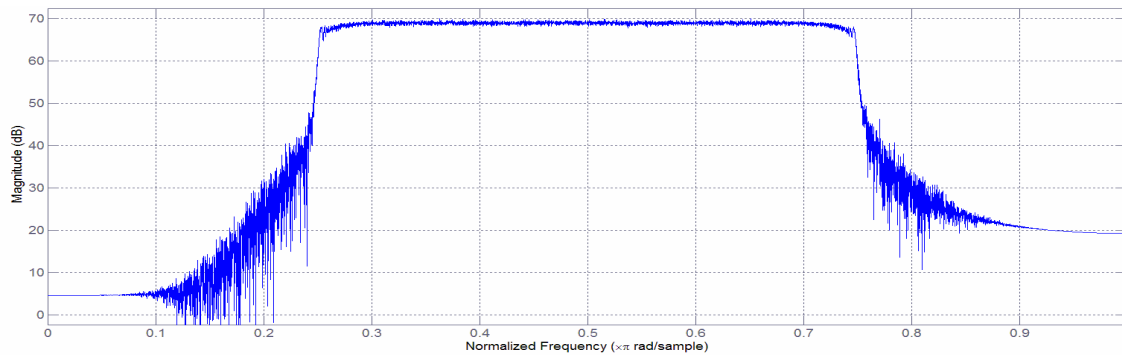
The jamming-to-signal ratio (JSR) for the i -th signal is defined as

$$JSR_i = 10 \log_{10} \left\{ \frac{P_{J,i}}{P_s} \right\} \quad (7)$$

Fig. 1 shows an example of a linear chirp jamming. The starting frequency is chosen as 2.046 MHz and after 4 ms, the instantaneous frequency is 6.138 MHz, i.e., the sweep rate $\beta=1.023$ GHz/sec. Fig. 2 illustrates an example of a convex chirp with $\beta=255.75$ GHz/sec². Fig. 3 depicts an example of a logarithmic chirp with $f_0=2.046$ MHz, $f_i(t_g)=6.138$ MHz, and $t_g=4$ ms.

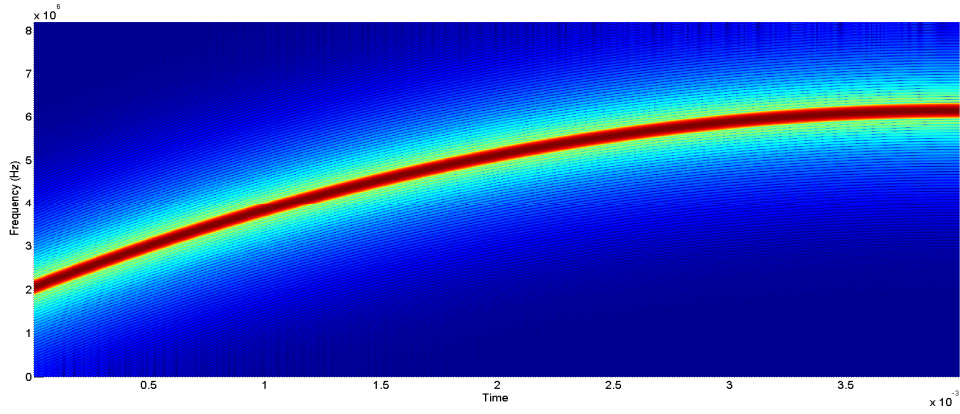


(a) time-frequency plot

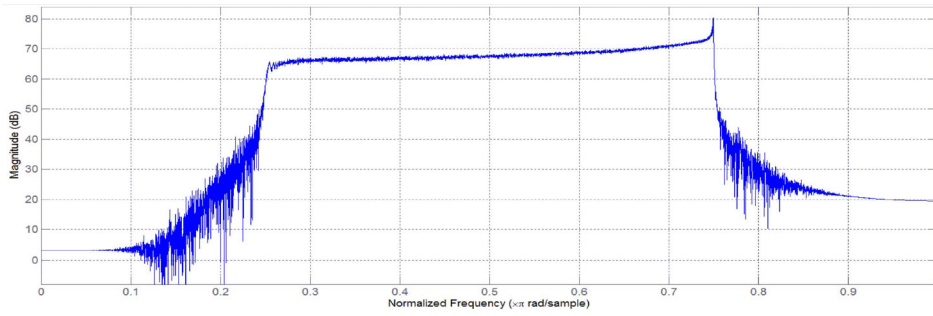


(b) magnitude spectrum of (5)

Fig. 1. An example of linear chirp jammer

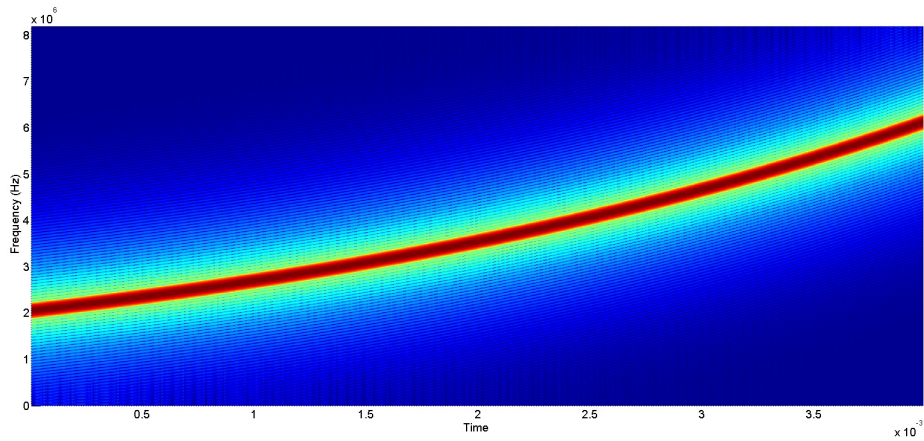


(a) time-frequency plot

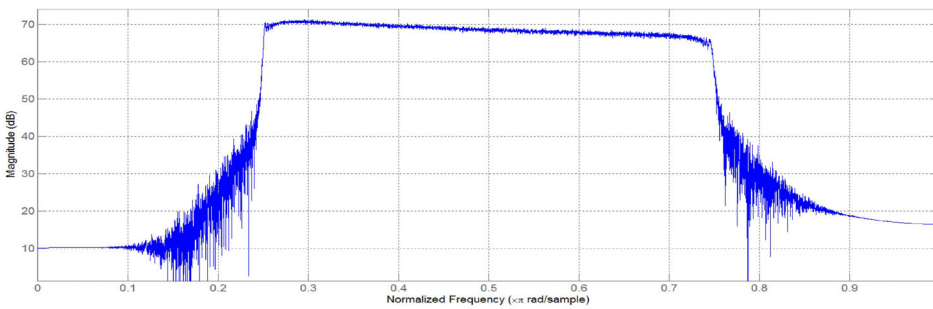


(b) magnitude spectrum of (5)

Fig. 2. An example of convex chirp jammer



(a) time-frequency plot



(b) magnitude spectrum of (5)

Fig. 3. An example of logarithmic jammer

3 Evaluation of the Impact of Jammers on the Acquisition and Tracking Blocks

3.1 Impaction on the Acquisition Block

Fig. 4 depicts a typical diagram of the acquisition function block, which performs a search for satellites in view. To quantify the quality of acquisition results, we define a signal-to-noise ratio (SNR) Γ as the performance metrics. The definition of Γ is the power ratio of the main peak value to other off-peak values after the received signals are despreading and can be expressed as

$$\Gamma = \frac{n[k]}{AVG_{n \neq k, k \pm 4} \{\eta[n]\}} \quad (8)$$

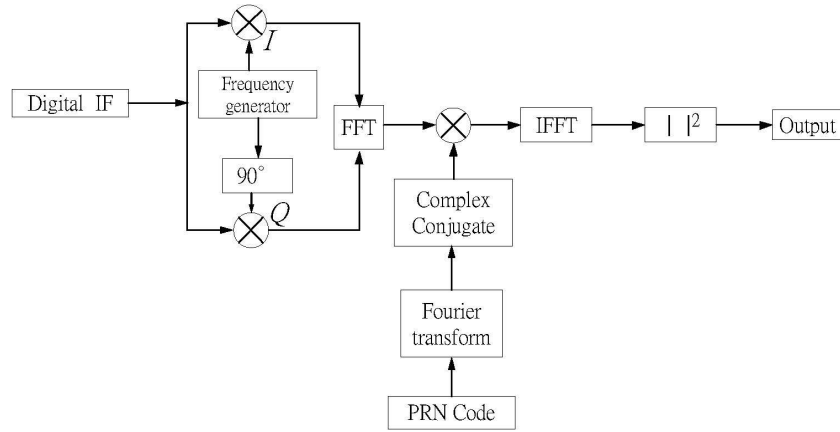


Fig. 4. A typical block diagram of acquisition block [1]

where $k = \arg \max_n \{\eta[n]\}$ denotes the index of the peak of the correlation output, $\{\eta[n]\}$ denotes the output of the circular cross-correlation between the input of the acquisition block and the spreading code, and $AVG \{\cdot\}$ the average operation. For a successful acquisition, we can obtain the estimation of a Doppler frequency \hat{f}_d and code phase offset $\hat{\tau}$ in (4) as shown in Fig. 5, where the coherent integration is 4 ms and the total integration time is 10 ms.

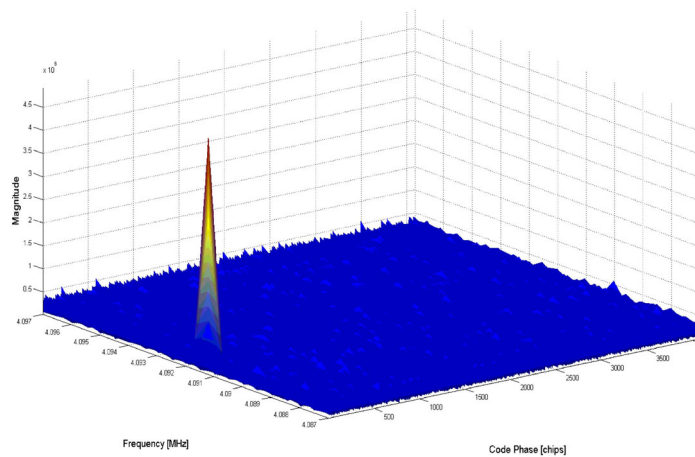


Fig. 5. An example of a successful acquisition

To evaluate the impact of jammers on the acquisition loop, we adopt the acquisition probability as the performance metric, which is defined as follows:

$$Pr_s \triangleq Pr \{ \hat{\tau} = \tau \cap \Gamma \geq \Gamma_{th} \} \quad (9)$$

where Γ is the SNR value and Γ_{th} is the pre-defined threshold.

Fig. 6. illustrates the procedure of calculating the Γ_{th} . Note that the input is only white noise. The resulting threshold $\Gamma_{th}=5.27$ dB when the corresponding the false alarm rate as 0.1%. The resulting acquisition probability for different types of chirp jammer are depicted in Fig. 7.

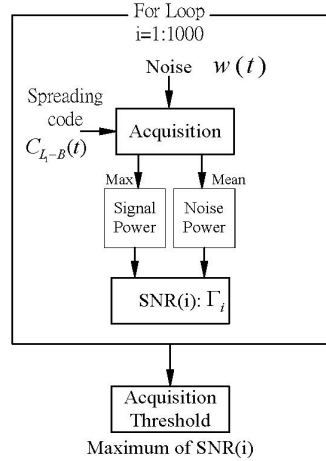
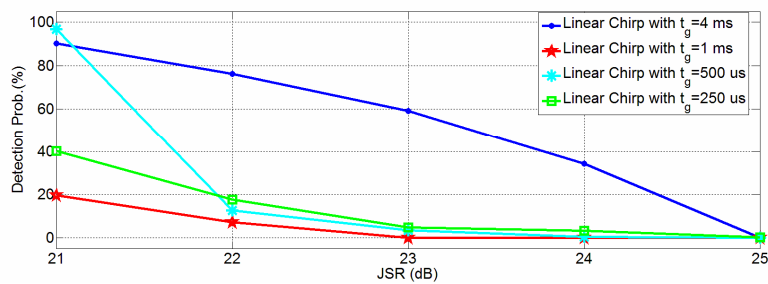
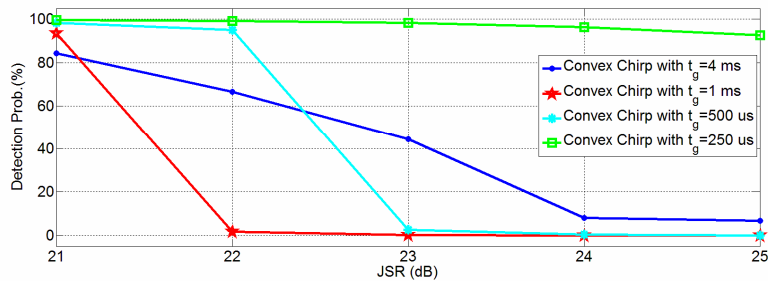


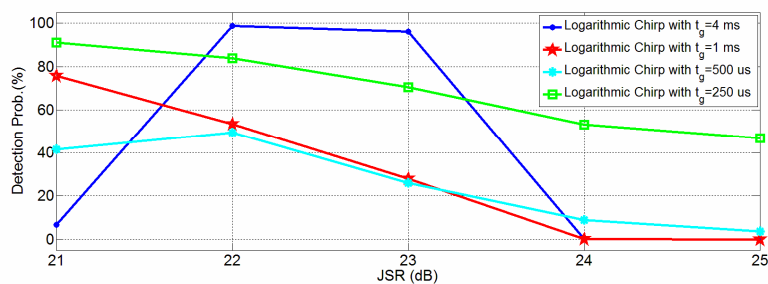
Fig. 6. The procedure of calculating the threshold



(a) linear



(b) convex



(c) logarithmic

Fig. 7. Resulting acquisition probability for different type of chirp jammer

3.2 Impaction on the Tracking Block

After the acquisition, the code phase and Doppler frequency of the acquired satellite are applied to initialize the tracking loops (Fig. 8). The loops are continuously updated every 4 ms so that the satellite and receiver dynamics can be tracked. For the carrier tracking loop, we can express the prompt output of the “integration and dump” on the in-phase arm as:

$$I_p[n] = LPF\{r[n] \cdot \cos(2\pi \hat{f}_{IF} n) \cdot C_{L_1-B}[n - \hat{\tau}]\} \approx D_{L_1-B}[n] \cdot \cos(\theta) \quad (10)$$

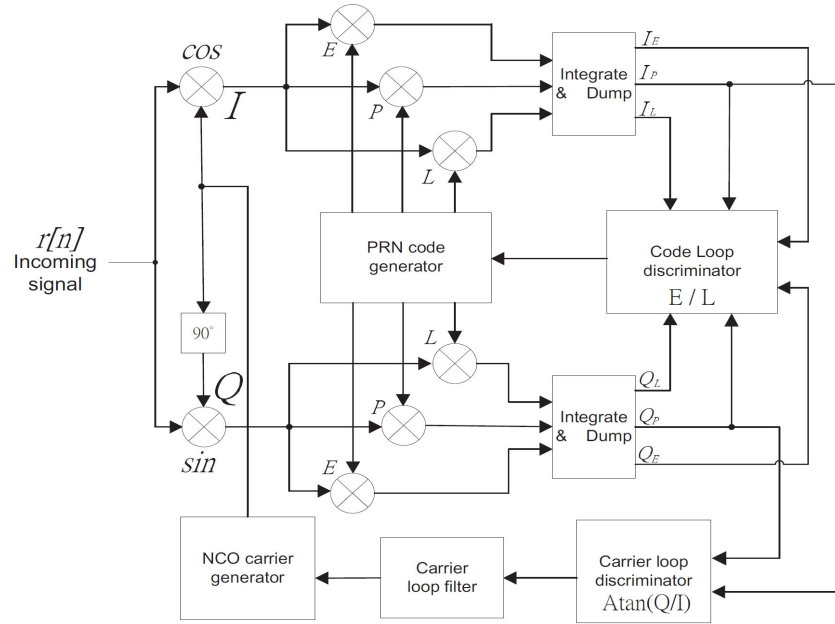


Fig. 8. A typical block diagram of tracking block [1]

Note that, we drop some constant terms in (10). Similarly, the prompt output of the “integration and dump” on the quadrature-phase arm can be expressed as:

$$Q_p[n] = LPF\{r[n] \cdot \sin(2\pi \hat{f}_{IF} n) \cdot C_{L_1-B}[n - \hat{\tau}]\} \approx D_{L_1-B}[n] \cdot \sin(\theta) \quad (11)$$

Therefore, the carrier-loop discriminator can extract the phase error. Therefore, the carrier-loop discriminator can extract the phase error $\hat{\theta}$ by

$$\hat{\theta}[n] = \arctan Q_p[n] / I_p[n] \quad (12)$$

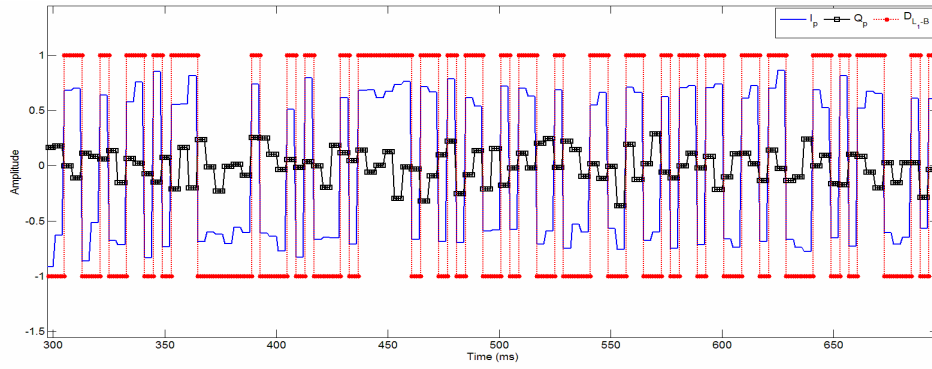
The estimated phase error then feeds to the numerically controlled oscillator (NCO) to adjust the frequency of \hat{f}_{IF} . By doing so, we can synchronize the carrier frequency with the transmitter.

For code tracking loop, we choose the non-coherent normalized early minus late power algorithm as the code phase discriminator. The output of the code phase discriminator can be expressed as

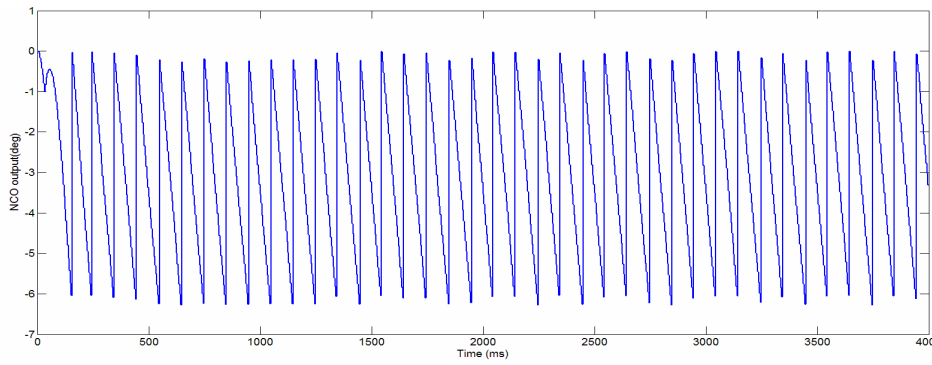
$$\Delta\tau = 0.5 \frac{E^2 - L^2}{E^2 + L^2} \quad (13)$$

where $E = \sqrt{I_E^2 + Q_E^2}$ and $L = \sqrt{I_L^2 + Q_L^2}$, Assumed that the satellite signals have been acquired, we evaluate the impaction of jammers on the tracking loops as illustrated in Fig. 9 and Fig. 10. The results show that the linear-chirp jammers have severely impaction on the tracking loops.

Impact of Jamming Attack on Galileo Receivers

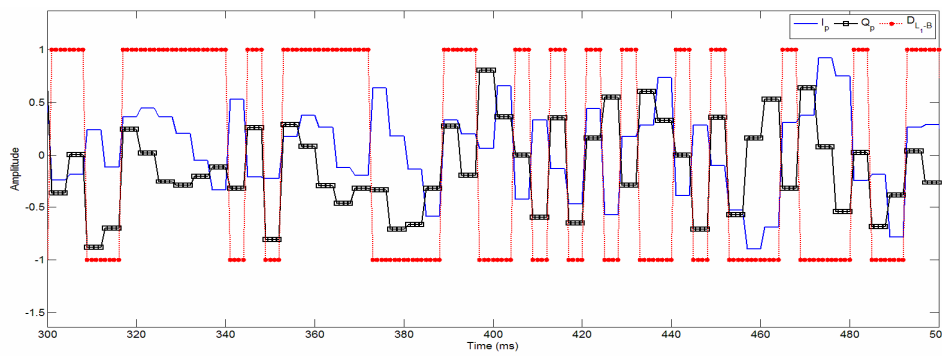


(a) outputs of in-phase and quadrature prompt arms and the corresponding navigation data

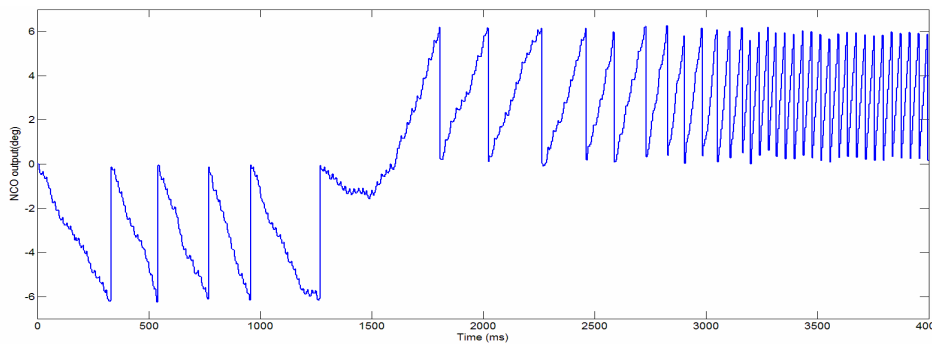


(b) NCO output

Fig. 9. The output of tracking loop when no jamming appears



(a) outputs of in-phase and quadrature prompt arms and the corresponding navigation data



(b) NCO output

Fig. 10. The output of tracking loop when a linear chirp with $JSR=23$ dB

4 Conclusions

We have numerically evaluated the impact of three kinds of chirp jammers, i.e., linear, convex, and logarithmic chirps, on the acquisition and tracking loops. The results indicate that Galileo receivers need to equip with jamming mitigation function to guarantee the required levels of QoS. Our future works are to design the anti-jamming algorithm to combat the chirp jammers for Galileo receivers.

Acknowledgements

This work was supported by the National Science Council, R.O.C., under Grant NSC102-2221-E-197-005.

References

- [1] E.D. Kaplan, *Understanding GPS: Principles and Applications*, 2nd ed., Arctec House, Norwood, MA, 2006.
- [2] I. Gupta, T.-H. Lee, K. Griffith, C.D. Slick, C. Reddy, M. Bailey, D. DeCarlo, Non-planar adaptive antenna arrays for GPS receivers, *IEEE Antennas Propag. Mag.* 52(5)(2010) 35-51.
- [3] Y. Zhang, M. Amin, Anti-jamming GPS receiver with reduced phase distortions, *IEEE Signal Process. Lett.* 19(10)(2012) 635-638.
- [4] D. Lu, R. Wu, H. Liu, Global positioning system anti-jamming algorithm based on period repetitive CLEAN, *IET Radar Sonar Navig.* 7(2)(2013) 164-169.
- [5] C. Palestini, R. Pedone, M. Villanti, G. Corazza, Integrated NAVCOM systems: Assisted code acquisition and interference mitigation, *IEEE Syst. J.* 2(1)(2008) 48-61.
- [6] D. Borio, L. Camoriano, L.L. Presti, Two-pole and multipole notch filters: a computationally effective solution for GNSS interference detection and mitigation, *IEEE Syst. J.* 2(1)(2008) 38-47.
- [7] Y.-R. Chien, Y.-C. Huang, D.-N. Yang, H.-W. Tsao, A novel continuous wave interference detectable adaptive notch filter for GPS receivers, in: *Proc. IEEE Global Telecommunications Conference (GLOBECOM)*, 2010.
- [8] N. Varshney, R. Jain, An adaptive notch filter for narrow band interference removal, in: *Proc. National Conf. Commun. (NCC)*, 2013.
- [9] Y.-R. Chien, Design of GPS anti-jamming systems using adaptive notch filters, *IEEE Syst. J.* 9(2)(2015) 451-460.
- [10] P.T. Capozza, B.J. Holland, T.M. Hopkinson, R.L. Landrau, A single-chip narrow-band frequency-domain excisor for a Global Positioning System (GPS) receiver, *IEEE J. Solid-State Circuits* 35(3)(2000) 401-411.
- [11] Z.-S. Wang, M. Lv, B. Tang, Paper application of partial coefficient update LMS algorithm to suppress narrowband interference in DSSS system, in: *Proc. Int. Conf. on Electronic Measurement & Instruments (ICEMI)*, 2009.
- [12] A.T. Balaei, A.G. Dempster, A statistical inference technique for GPS interference detection, *IEEE Trans. Aerosp. Electron. Syst.* 45(5)(2009) 1499-1509.
- [13] Y.-R. Chien, Hybrid successive continuous wave interference cancellation scheme for global positioning system receivers, *The Journal of Engineering* 1(2013) 1-8.
- [14] D. Borio, L. Camoriano, S. Savasta, L. Lo Presti, Time frequency excision for GNSS applications, *IEEE Syst. J.* 2(1)(2008) 27-37.
- [15] S. Savasta, L. Lo Presti, M. Rao, Interference mitigation in GNSS receivers by a time-frequency approach, *IEEE Trans. Aerosp. Electron. Syst.* 49(1)(2013) 415-438.

- [16] C. Togni, R. Pedone, M. Villanti, M. Iubatti, G. Corazza, Time-frequency power adaptive interference mitigation for galileo L1 band receivers, in: Proc. Mobile and Wireless Communications Summit, 2007.
- [17] R.H. Mitch, R.C. Dougherty, M.L. Psiaki, S.P. Powell, B.W. O'Hanlon, Signal characteristics of civil GPS jammers, in: Proc. ION GNSS, 2011.
- [18] D. Borio, C. O'Driscoll, J. Fortuny, GNSS jammers: Effects and countermeasures, in: Proc. 6th ESA Workshop on Satellite Navigation Technologies and European Workshop on GNSS Signals and Signal Processing (NAVITEC), 2012.
- [19] R.H. Mitch, M.L. Psiaki, S.P. Powell, B.W. O'Hanlon, Signal acquisition and tracking of chirp-style GPS jammers, in: Proc. ION GNSS, 2013.
- [20] D. Borio, C. O'Driscoll, J. Fortuny, Jammer impact on Galileo and GPS receivers, in Proc. Int. Conf. Localization and GNSS (ICLGNSS), 2013.
- [21] Y.-R. Chien, P.-Y. Chen, S.-H. Fang, Novel anti-jamming algorithm for GNSS receivers using wavelet-packet-transform-based adaptive predictors, IEICE TRANSACTIONS on Fundamentals of Electronics, Communications and Computer Sciences 100(2)(2017) 602-610.